Environmental Science and Pollution Research (2023) 30:1096–1115
https://doi.org/10.1007/s11356-022-21987-0

RESEARCH ARTICLE

Compressive strength prediction of high-strength oil palm shell lightweight aggregate concrete using machine learning methods

Saeed Ghanbari[1] · Amir Ali Shahmansouri[1] · Habib Akbarzadeh Bengar[1] · Abouzar Jafari[2]

Received: 18 January 2022 / Accepted: 8 July 2022 / Published online: 1 August 2022

Abstract
Promoting the use of agricultural wastes/byproducts in concrete production can significantly reduce environmental effects and contribute to sustainable development. Several experimental investigations on such concrete's compressive strength (f_c) and behavior have been done. The results of 229 concrete samples made by oil palm shell (*OPS*) as a lightweight aggregate (*LWA*) were used to develop models for predicting the f_c of the high-strength lightweight aggregate concrete ($HS-LWAC$). To this end, gene expression programming (*GEP*), adaptive neuro-fuzzy inference system (*ANFIS*), artificial neural network (*ANN*), and multiple linear regression (*MLR*) are employed as machine learning (*ML*) and regression methods. The water-to-binder (W/B) ratio, ordinary Portland cement (*OPC*), fly ash (*FA*), silica fume (*SF*), fine aggregate (*Sand*), natural coarse aggregate (*Gravel*), *OPS*, superplasticizer (*SP*) contents, and specimen age are among the nine input parameters used in the developed models. The results show that all *ML*-based models efficiently predict the $HS-LWAC$'s f_c, which comprised *OPS* agricultural wastes. According to the results, the *ANN* model outperformed the *GEP* and *ANFIS* models. Moreover, an uncertainty analysis through the Monte Carlo simulation (MCS) method was applied to the prediction results. The growing demand for sustainable development and the crucial role of eco-friendly concrete in the construction industry can pave the way for further application of the developed models due to their superior robustness and high accuracy in future codes of practice.

Keywords Agricultural waste · Lightweight aggregate concrete · High-strength concrete · Strength prediction · Machine learning

Introduction

The demand and cost of construction materials are increasing due to the world's rapidly growing population (Shadmani et al. 2018). The ever-growing demand for natural resources to meet the demand of the market and economic growth has resulted in a detrimental impact on the environment and a lack of raw materials (Saberian et al. 2021). In some countries, agricultural wastes/byproducts can be harmful to the ecosystem if these wastes/byproducts are not recycled/pretreated (Sodhi et al. 2021). Either fully or partially use of solid agricultural wastes/byproducts, particularly for concrete production, as a suitable replacement for raw materials has been studied by many researchers (e.g., Aslam et al. 2016a, Chinnu et al. 2021, Rashad 2016, Shafigh et al. 2014b). The reported results showed that this replacement is a promising approach to achieving sustainable development (Islam et al. 2016). Among agricultural wastes/byproducts, oil palm shell (*OPS*) (see Fig. 1) that is abundantly available in large quantities in tropical countries such as Indonesia, Malaysia, and Thailand can be easily and efficiently used as a construction material for concrete production (Hamada et al. 2020).

Every year, around 4.56 million tons of *OPS* wastes are produced, according to the current statistics (Shafigh et al.

Responsible Editor: Philippe Garrigues

Habib Akbarzadeh Bengar
h.akbarzadeh@umz.ac.ir

Saeed Ghanbari
saeed.ghanbari@stu.umz.ac.ir

Amir Ali Shahmansouri
aa.shahmansouri@stu.umz.ac.ir

Abouzar Jafari
a_jafari@sjtu.edu.cn

[1] Department of Civil Engineering, University of Mazandaran, Babolsar, Iran

[2] University of Michigan and Shanghai Jiao Tong University Joint Institute, Shanghai Jiao Tong University, Shanghai, China

Fig. 1 Shape of *OPS* aggregate (Mo et al. 2015, 2018)

2012b). The advantages of utilizing *OPS* waste as a lightweight aggregate (*LWA*) in the fabrication of lightweight aggregate concrete (*LWAC*) have been reported by many researchers (e.g., Ahmad Zawawi et al. 2020, Aslam et al. 2016c). Moreover, numerous studies have proven that using *OPS* decreases the need for coarse material made from natural resources while improving sustainability due to lower pollution levels. The produced structural concrete using *OPS* as an *LWA* showed to have an acceptable compressive strength (f_c) at 28 *days*, and 20–30% lower density (compared with normal weight concrete (*NWC*)) according to the existing literature (Aslam et al. 2016b; Shafigh et al. 2014c). Furthermore, in terms of flexure and bond strength, the *OPS* concrete displays good structural performance (Johnson Alengaram et al. 2011; Teo et al. 2006; Thomas et al. 2017).

The phrase "lightweight concrete (LWC)" refers to concrete that has an oven-dried density of less than 2000 kg/m^3 and can be manufactured from various natural aggregates. The phrase structural LWC, on the other hand, refers to concrete that has an oven-dried density of less than 2000 kg/m^3 and is made using coarse LWA s with normal fine or fine and coarse LWA s. A high-strength lightweight aggregate concrete ($HS-LWAC$) has a compressive strength of $34-69$ MPa, and a dry density of less than 2000 kg/m^3 (Mehta and Monteiro 2014). Generally, to obtain the desirable high-strength in LWC, a water-to-cement (W/C) ratio of less than 0.45 is used to obtain the desirable high-strength in LWC (Hoff 2002). High-strength concrete (HSC) with normal weight could generally achieve the cylindrical compressive strength of 40 MPa and above. It was used in the construction industry (in the year 1960) with a compressive strength of up to 50 MPa. HSC with normal density, on the other hand, has a compressive strength of above 41 MPa, according to American Concrete Institute reports (American Concrete Institute 1997). According to Mehta and Monteiro (Mehta and Monteiro 2014), a concrete with good quality LWA and a high cement content may reach compressive strengths of 40 to 50 MPa.

Previous research has demonstrated that in concrete production, agricultural wastes/byproducts could replace normal coarse aggregate to produce structural LWC (Alengaram et al. 2013). Shafigh et al. (2011b) proposed utilizing OPS to make $HS-LWAC$ by crushing big OPS shells for performing this process. The reported physical bond between crushed OPS shell and hydrated cement paste was reported strong and the shell was quite hard. The compressive strength reported in this investigation was around 53 and 56 MPa in 28 and 56 *days*, respectively. Furthermore, it was reported that *Grade* 30 *OPS* concrete could be manufactured without the use of any cementitious material. Another research demonstrated that *OPS* concretes with a $28-day$ f_c of around $43-48MPa$ and a dry density at around $1870-1990$ kg/m^3 can be produced both with and without limestone powder (Alengaram et al. 2013; Shafigh et al. 2014c). To ensure the higher compressive capacity $OPS-LWAC$, generally, the compressive strength (f_c) is needed to be evaluated as the determinative factor. As a result, accurate and reliable compressive strength prediction of $OPS-LWAC$ before using it is critical for making crucial judgments (Zhang et al. 2020).

Nowadays, linear/nonlinear regression techniques are widely used for predicting concrete characteristics (Sadrmomtazi et al. 2019). However, there are few regression models for estimating *OPS* concrete compressive strength. Furthermore, utilizing empirical-based models, obtaining an accurate regression equation is quite challenging (Chou and Pham 2013). Among newly developed machine learning (ML) approaches, gene expression programming (GEP) (Ferreira 2001), adaptive neuro-fuzzy inference system ($ANFIS$) (Jang 1993), and artificial neural network (ANN) (Hornik et al. 1989) have been widely employed to formulate the conventional statistical methods/models (i.e., regressions) (e.g., Farooq et al. 2021, Latif 2021a). In order to distinguish the relationship between input factors and $HS-OPS-LWAC$'s f_c, therefore, in this study, the above-mentioned ML approaches are used.

To the best of the authors' knowledge, no ML -based model exists for estimating/predicting the

HS – OPS – LWAC compressive strength. Therefore, this study uses a comprehensive database collected from the literature to predict the compressive strength of the *HS – OPS – LWAC*, by employing *ANN*, *ANFIS*, and *GEP* approaches. After that, the employed approaches' efficiency, performance, and predictive validity are compared using multiple statistical approaches. In the "Research methodology" section, the employed *ML* and regression methods will be explained. The "Modeling procedure" section is about compiling the collected dataset, and in the "Results and discussion" section, the modeling procedure is further described. Evaluating and comparing the efficiency and performance of the proposed models are further discussed in the "Conclusions" section.

Research methodology

In this section, first, the data collected on *HS – LWAC* mix designs were explained and descriptive and statistical information about this data was given. In the following, comprehensive explanations were given about the used regression and *ML* methods including *MLR*, *GEP*, *ANFIS*, and *ANN*.

Data collection

To predict the compressive strength of *HS – LWAC*, a dataset including 229 experimental data records was compiled from previous research studies (Alengaram et al. 2008a, b; Aslam et al. 2015, 2016b, c, 2017, 2018; Farahani et al. 2017a, b; Maghfouri et al. 2017, 2018, 2020; Muthusamy et al. 2020; Shafigh et al. 2011a, b, 2012a, b, c, 2013a, b, 2014a, c, 2016, 2018; Yahaghi et al. 2016). This dataset included information such as the content of fine aggregate (*Sand*), natural coarse aggregate (*Gravel*), ordinary Portland cement (*OPC*), fly ash (*FA*), silica fume (*SF*), superplasticizer (*SP*), and *OPS*, as well as the water-to-binder (W/B) ratio. It also included the age and compressive strength (f_c) values of the test specimens. Since the aim of this study was the prediction of the compressive strength of *HS – LWAC*, the 28 – *day* f_c of all specimens were higher than 34*MPa*. The modeling input and output variables histograms are displayed in Fig. 2.

In Table 1, the descriptive statistics of the input and output variables are provided. As can be seen in this table, for specimens with ages of 1 to 120 *days*, the compressive strength varies from 13.71 to 84.45 *MPa*. Of all the specimens, 76 contained no gravel, which allowed the

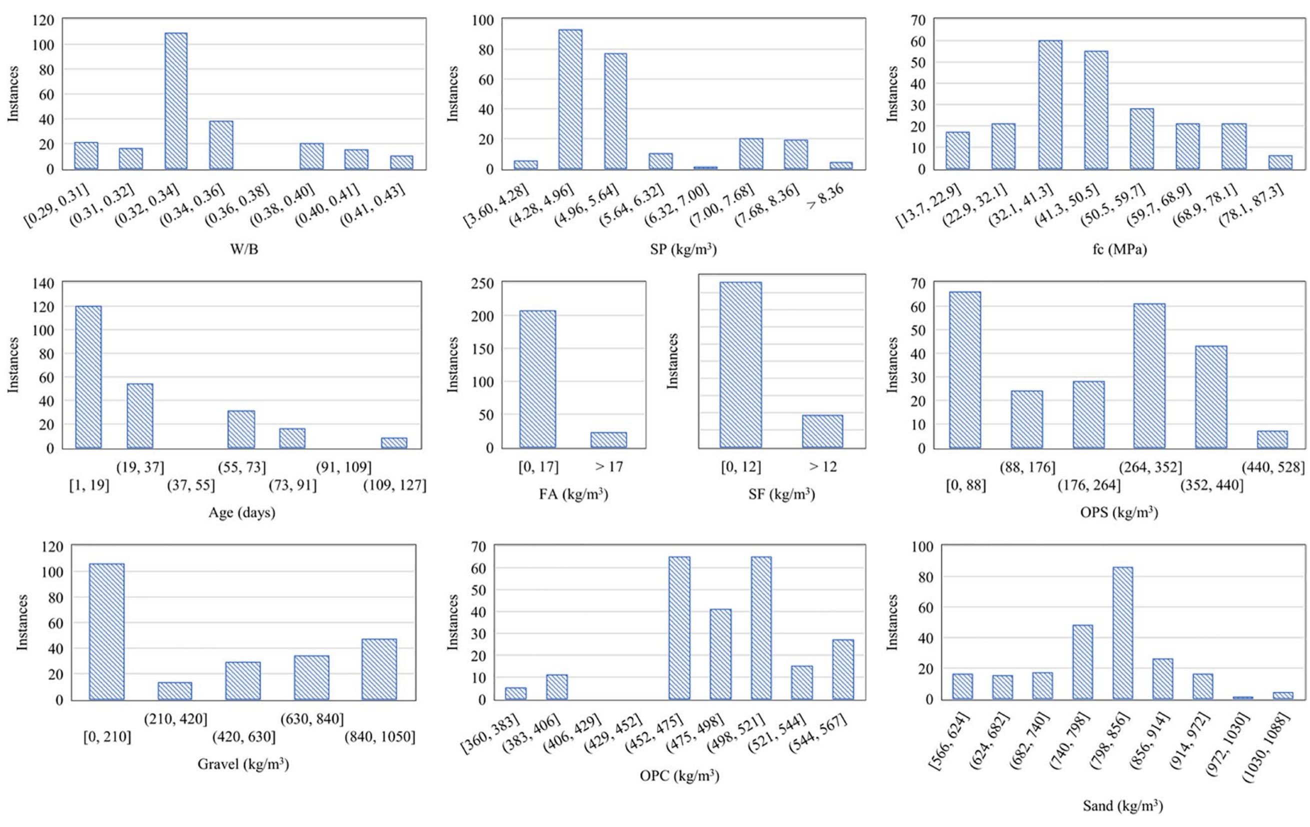

Fig. 2 Histograms of the database parameters

Table 1 Descriptive statistics of the input and output variables

Statistical indicator	$OPC(kg/m^3)$	$FA(kg/m^3)$	$SF(kg/m^3)$	$^{W}/_{B}$	$SP(kg/m^3)$	$S(kg/m^3)$	$G(kg/m^3)$	$OPS(kg/m^3)$	$Age(days)$	$f_c(MPa)$
Mean	491.2	8.1	8.9	0.3	5.5	793.4	395.1	222.4	26.6	46.2
Median	495	0	0	0.34	5	812	348	243	7	42.8
Mode	500	0	0	0	5	812	0	0	28	74
Minimum	360	0	0	0.29	3.6	566	0	0	1	13.7
Maximum	550	165	60	0.4	9.4	1050	963	451.5	120	84.5
Std	40.2	30.5	20.5	0.0	1.2	101.1	362.0	154.6	31.4	16.0
Kurtosis	2.5	17.0	1.6	0.7	1.3	0.5	−1.6	−1.3	1.3	−0.4
Skewness	−1.14	4.18	1.89	0.57	1.46	−0.36	0.24	−0.25	1.41	0.40

investigation of the effect of the 100% substitution of *OPS*. The highest content of *OPS* (i.e., 451.5 kg/m^3) decreased the specific gravity of the concrete to 1900 kg/m^3 (see Table 1). However, in designs without *OPS* where the coarse aggregate was entirely gravel, the specific gravity values were greater than 2228 kg/m^3. In 22 mix designs, in addition to *OPC*, *FA* was also used as the binder. The highest content of *FA* was 165 kg/m^3, and the *OPC* content in

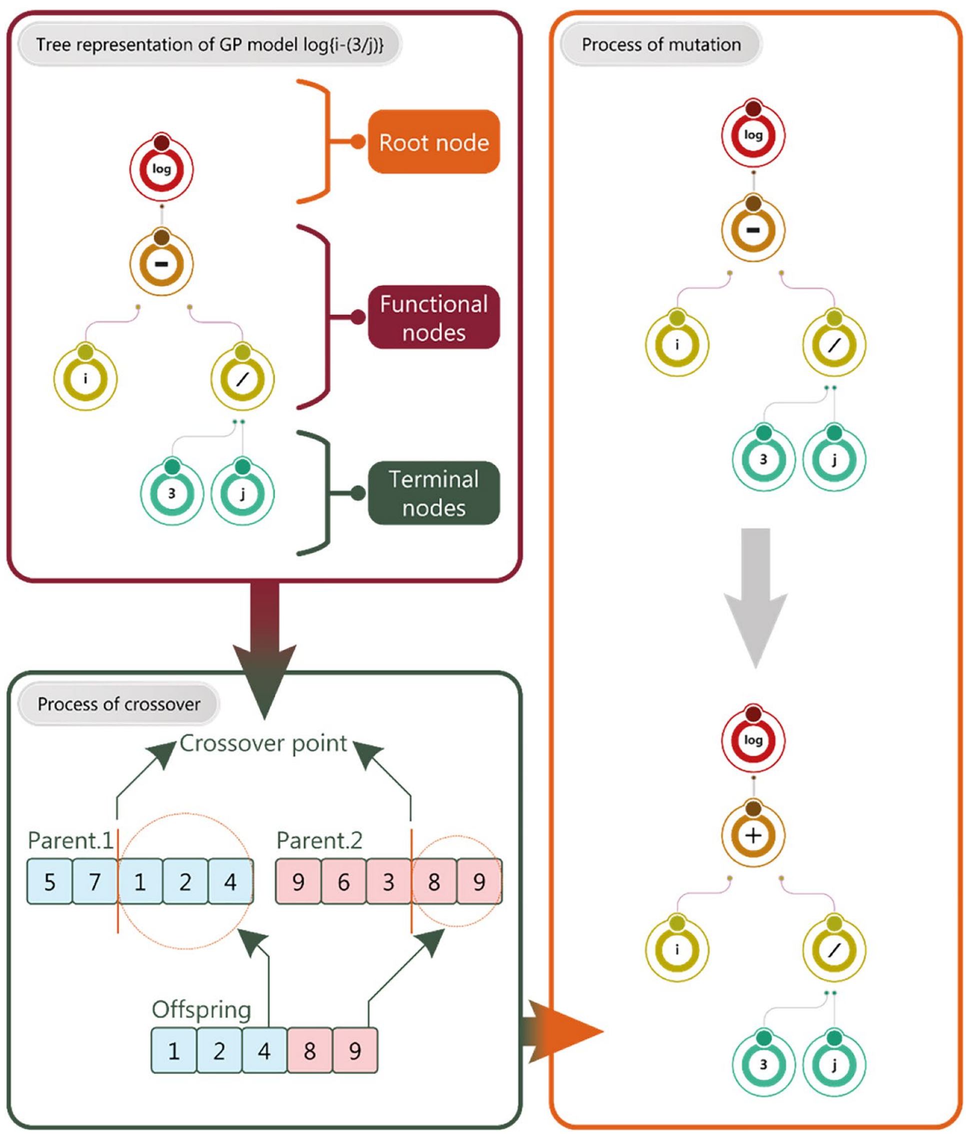

Fig. 3 A typical *GEP* model, the algebraic equation, and its corresponding *ET* with phenotype, along with the crossover and mutation processes

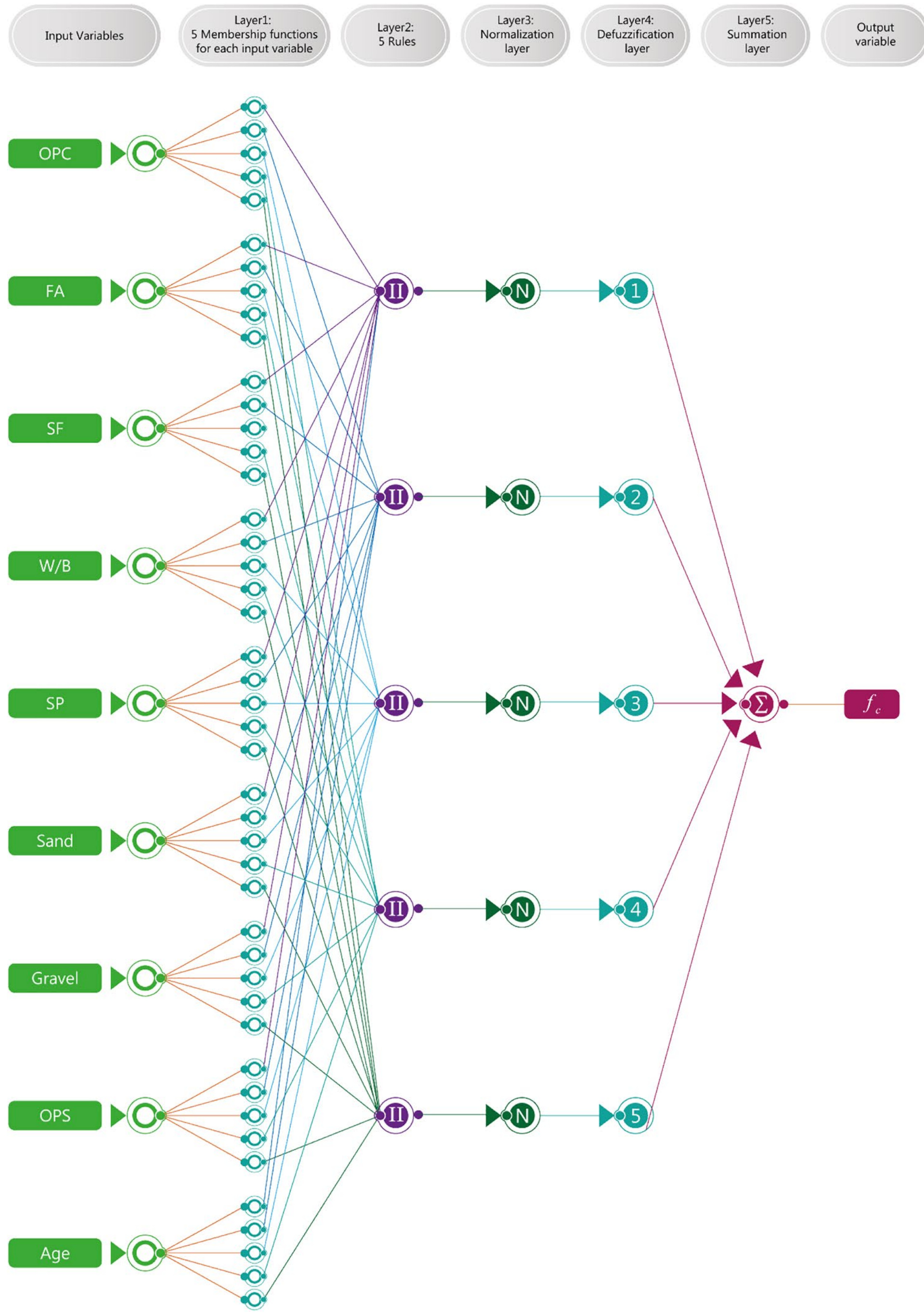

Fig. 4 The employed *ANFIS* schematic with the defined parametric conjunction operations

this design was 385 kg/m^3. In addition, the lowest content of *FA* among these 22 designs was 22.85 kg/m^3, and the *OPC* content in the corresponding design was 388 kg/m^3. The use of *FA* slightly increased the $28-day\ f_c$. On the other hand, it had a positive effect on the drying shrinkage of concrete and improved concrete durability (Mo et al. 2020). Moreover, in 37 mix designs, *SF* was also used as partial replacement of cement, with the highest content of 60 kg/m^3 and lowest content of 45.7 kg/m^3. The mix designs containing *SF* had higher compressive strength values compared with those without *SF*. The reason for this may be the fineness of *SF* particles and the reaction of silicon dioxide with calcium hydroxide.

Multiple linear regression approach

Regression approaches predict how a dependent variable varies by changing independent variable(s). Multiple linear regression (*MLR*) (Andrews 1974), often known as multiple regression, is an approach that statically predicts the result of

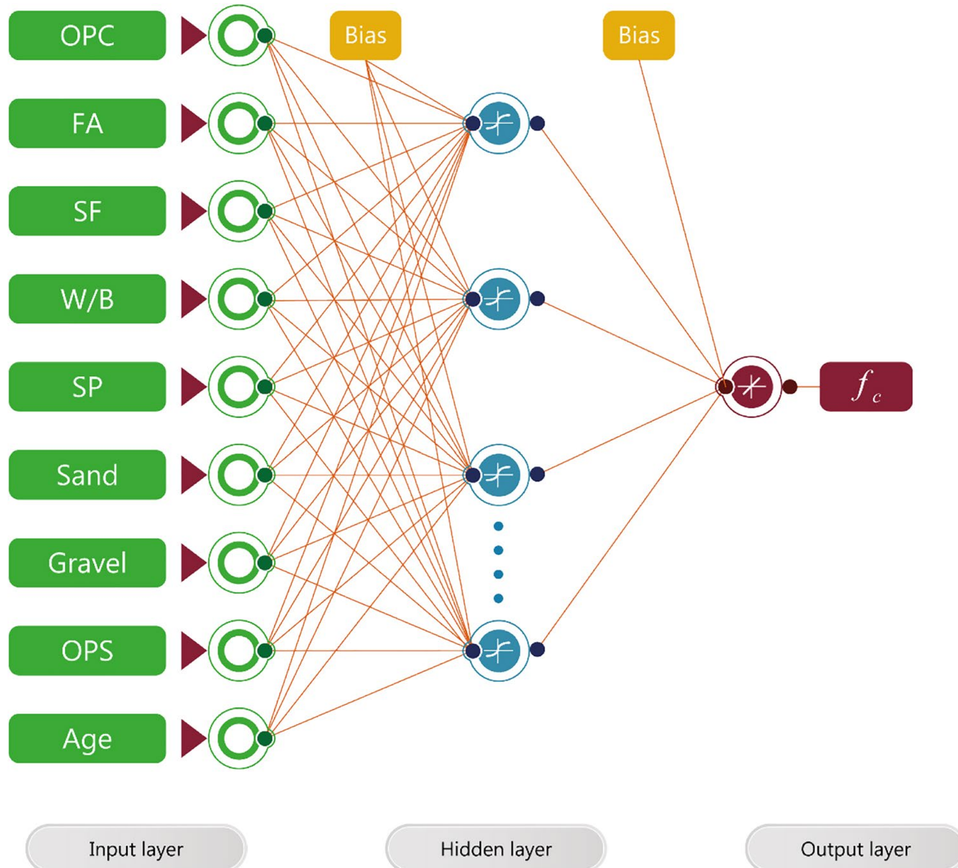

Fig. 5 The architecture of the used feed-forward *ANN* with nine inputs

a response variable by combining multiple explanatory variables/parameters. Since *MLR* approach contains more than one explanatory variable (independent), multiple regression is essentially an ordinary least-squares (*OLS*) regression extension that can be expressed as follows:

$$y = \beta_0 + \beta_1 x_1 + \cdots + \beta_n x_n + \varepsilon \quad (1)$$

where y is the dependent variable predicted value; β_0 is the value of y-intercept (y value considering all other parameters are set to zero); β_1 and β_n are the regression coefficient of the first and last independent variable, respectively; x_1 and x_n are the first and last independent variable, respectively; and ε is the model error. *MLR* approaches calculate three factors to obtain the best-fit line for each independent (explanatory) variable including (1) the regression method coefficients that lead to the least overall model error, (2) the entire model's t-statistic, and (3) the p-value that corresponds to the entire model's t-statistic. The model's t-statistic and p-value are then calculated for each regression coefficient.

Gene expression programming approach

Gene expression programming (*GEP*) method (Ferreira 2001), based on Darwin's theory of evolution and Mendel's genetic theory, is one of the most logically appealing computational intelligence formalisms. There are two languages in *GEP* algorithms including the gene and the expression trees (*ET* s) languages. Comprehending one of these languages requires knowledge of the sequence/structure of the other (Ferreira 2002). The following are the basic processes involved in standard/typical *GEP* modeling. *GEP* modeling starts with a random chromosome's generation for specific numbers, followed by the introduction of the chromosomes using *Karva* language (i.e., representing symbols). A chromosome or gene usually has a head and a tail; the chromosome's head composed of some terminal symbols or a function, whereas only terminal symbols form the chromosome's tail (Shishegaran et al. 2020). In a *GEP* model, the sub-*ET* s' number is determined by the head size, which takes into account each parameter's complexity. The lengths of the chromosomes are fixed and may be easily converted/transformed into an algebraic equation, as seen in Fig. 3.

Each *GEP* gene has a collection of terms (i.e., a fixed-length list) that are adapted from the function set, including arithmetic operations (+, −, ×, ÷), and functions such as *Boolean* logic (*AND*, *OR*, *NOT*, etc.), mathematical (*cos*, *sin*, *ln*), conditional (*IF*, *THEN*, *ELSE*), and so on. The chromosomes are then represented by *ET* s that come in various sizes and shapes. The major genetic operators

Table 2 Statistical parameters for each *GEP* model

Models	Phase	R^2	*RMSE*	*MAE*
*GEP*1	Training	0.848	6.399	4.798
	Validation	0.827	8.412	6.718
*GEP*2	Training	0.814	6.944	5.462
	Validation	0.776	9.016	6.656
*GEP*3	Training	0.886	5.496	4.049
	Validation	0.893	6.771	5.246
*GEP*4	Training	0.880	5.370	3.642
	Validation	0.892	6.126	4.313
*GEP*5	Training	0.868	5.467	4.077
	Validation	0.865	4.714	5.380
*GEP*6	Training	0.877	5.401	4.008
	Validation	0.892	6.238	4.954
*GEP*7	Training	0.851	5.851	4.180
	Validation	0.859	7.036	5.484
*GEP*8	Training	0.898	5.080	3.860
	Validation	0.901	6.501	5.245
*GEP*9	Training	0.867	6.499	4.500
	Validation	0.863	8.405	6.489
*GEP*10	Training	0.837	6.694	4.798
	Validation	0.845	8.267	6.194
*GEP*11	Training	0.811	6.549	4.788
	Validation	0.841	7.283	5.647
*GEP*12	Training	0.882	5.788	4.204
	Validation	0.890	7.438	5.519
*GEP*13	Training	0.847	5.915	4.404
	Validation	0.839	7.374	5.439
*GEP*14	Training	0.849	6.031	4.884
	Validation	0.849	7.610	6.000
*GEP*15	Training	0.874	5.372	4.059
	Validation	0.878	6.397	5.288
*GEP*16	Training	0.813	6.498	4.781
	Validation	0.803	8.154	6.116
*GEP*17	Training	0.890	4.999	4.021
	Validation	0.840	7.313	5.452
***GEP*18**	**Training**	**0.897**	**4.859**	**3.946**
	Validation	**0.898**	**6.082**	**4.860**
*GEP*19	Training	0.860	5.675	4.552
	Validation	0.861	7.043	5.853
*GEP*20	Training	0.862	5.665	4.617
	Validation	0.836	7.606	6.180

Bold is the best model

of crossover, transposition, mutation, and recombination (one-point, two-point, and gene recombination) are then conducted on the chromosomes, in line with their ratios (Londhe et al. 2021). The process of mutation and crossover and a typical *ET* are displayed in Fig. 3. It is also worth noting that the *ET* is represented in *Karva* notation/*K*-expression. Reaching a suitable solution or highest/enough generation number (the stop condition), the whole process will stop. If the maximum iteration or preferred fitness value termination requirements are not fulfilled, the Roulette wheel method, ranking/tournament selection, elite strategy, etc., is used. This procedure would be repeated until the optimal/best solution was found or for a defined generation number.

Adaptive neuro-fuzzy inference system approach

Adaptive neuro-fuzzy inference system (*ANFIS*) (Jang 1993) is an appealing computational intelligence modeling technique that combines the *ANN* learning capability with the fuzzy logic reasoning capability. *ANFIS* has a better estimate ability and is a better alternative for processing nonlinear complicated problems more precisely (Gholizadeh et al. 2022). *ANFIS* algorithms learn from the collected data for training with any complicated mathematical model, then maps out the obtained solutions onto a fuzzy inference system (*FIS*) (Saradar et al. 2020).

Using *ANFIS* tool in *MATLAB*, a typical *FIS* consists of many phases, one of which is the introduction of inputs to aid in fuzzy sets fuzzification according to the linguistic rules activation. Following that, particular rules/guidelines are either created by specialists or can be derived from numerical data available in the literature. The next stage is inference, which involves mapping fuzzy sets according to set rules. Finally, the fuzzy sets are defuzzified, resulting in the final output values. In other words, the *ANFIS* technique is made up of five key steps: (1) dataset; (2) development of *ANFIS*; (3) variable setup; (4) training and then validation; (5) obtaining results. In addition, the architecture of *ANFIS* for the nine input variables (*OPC*, *FA*, *SF*, W/B, *SP*, *Sand*, *Gravel*, *OPS*, and *Age*) is shown in Fig. 4. More detail regarding the method and development of *ANFIS* can be found in Mohammadi Golafshani et al. (2021).

Artificial neural network approach

Artificial neural networks (*ANN* s) (Hornik et al. 1989) are computer algorithms that can accurately and effectively forecast and categorize data processing difficulties. They are mathematical models based on the properties of biological neuron networks that are similar to the human brain (Liu et al. 2021). *ANN* s have a layered structure with a variety of processing elements (*PE* s) and arranged nodes, including (1) an input layer which composed of independent variables, (2) a hidden layer/s which is composed of several hidden variables, also known as hidden neurons, and (3) an output layer which contains the outputs/target values (Ahmed et al. 2022) (see Fig. 5).

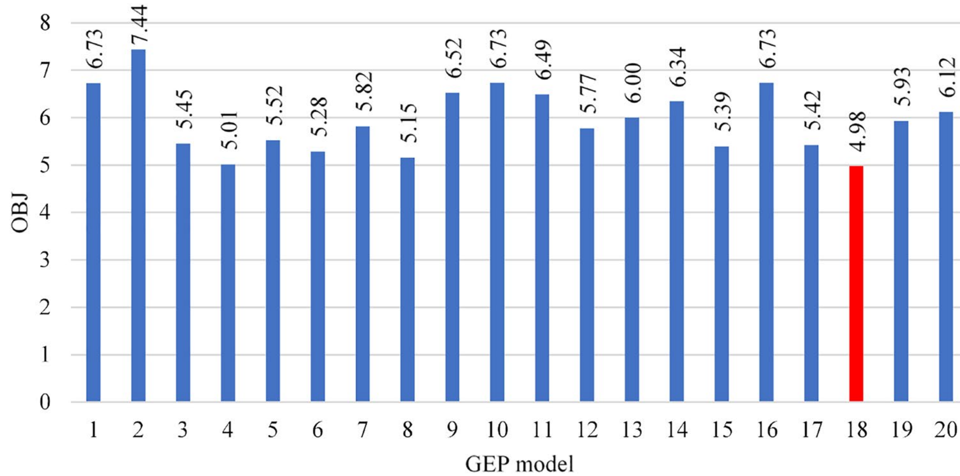

Fig. 6 The *OBJ* values for all *GEP* models (red bar is the best)

The influential factors in the research were chosen as inputs to produce the respective outputs compressive strength of concrete (f_c), as shown in Fig. 5. Each input from the preceding layer (*OPC*, *FA*, *SF*, *W*/*B*, *SP*, *Sand*, *Gravel*, *OPS*, *Age*) is multiplied by an appropriate weight factor (weight connection) in the hidden layer. A threshold value is added to each node's weighted input signals summations. The combined input then goes through a transfer phase that includes a non-linear transfer function (*TF*) (Latif 2021b).

Linear, stepped, logistic sigmoid, and hyperbolic tangent sigmoid are the most widely employed activation functions (*AF* s) in *ANN* s. The output of one *PE* serves as the input for the subsequent *PE*. Each neuron in the hidden and output layers performs a logistic function as an *AF* (Parsaie et al. 2021). *AF* is a crucial essential property of neural networks, and it has a substantial influence on the *ANN* model performance and efficiency; therefore, choosing and employing the viable and workable *AF* is critical (Ehteram et al. 2021). In this study, to increase the performance and accuracy of the obtained output, *AF* of Backpropagation neural network (*BPNN*) and *PURELIN* are employed. *BPNN*'s output is within the range of −1 to +1 and is related to a bipolar *Sigmoid* which is employed in the hidden layer. *PURELIN* is a linear *AF* which is employed in the output layer. The number of neurons in each layer and each *TF* increases as a result of using these *AF* s. Therefore, for the training dataset, using *BPNN* and *PURELIN* improves the statistical indices; however, it decreases the accuracy for testing the dataset and validation (Ghadami et al. 2021).

The training/learning phase begins when the *ANN* starts propagating the collected data (information) from the input layer, and the weight factors (connections) are modified according to the specified rules for finding the best combination of weights to create the least amount of error possible (Shahmansouri et al. 2021). The trained model is then verified using a new testing set. More detail regarding the *ANN* approach and its development can be found in Shahmansouri et al. (2022).

Table 3 *GEP* setting parameters used for *GEP*18

Parameters	Value/setting
Head size	12
Chromosome	40
Number of genes	4
Mutation rate	0.044
Inversion rate	0.1
Transposition rate	0.1
Linking function	Addition
Operators used	+, −, ∗, /, *exp*, *sin*, *cos* ,*atan*
Fitness function	*RRSE*
Constant per gene	1

Modeling procedure

To model the compressive strength of *HS* − *LWAC*, nine input variables introduced and characterized in the previous section, together with an output variable being the compressive strength, were considered. The total number of experimental data points used in the modeling was 229 in all the methods.

Data curation

For *ANN* and *ANFIS* modeling approaches, considering the input and output domains' differences, all input variables were normalized to increase the accuracy and speed of the models (Shahmansouri et al. 2022). To this end,

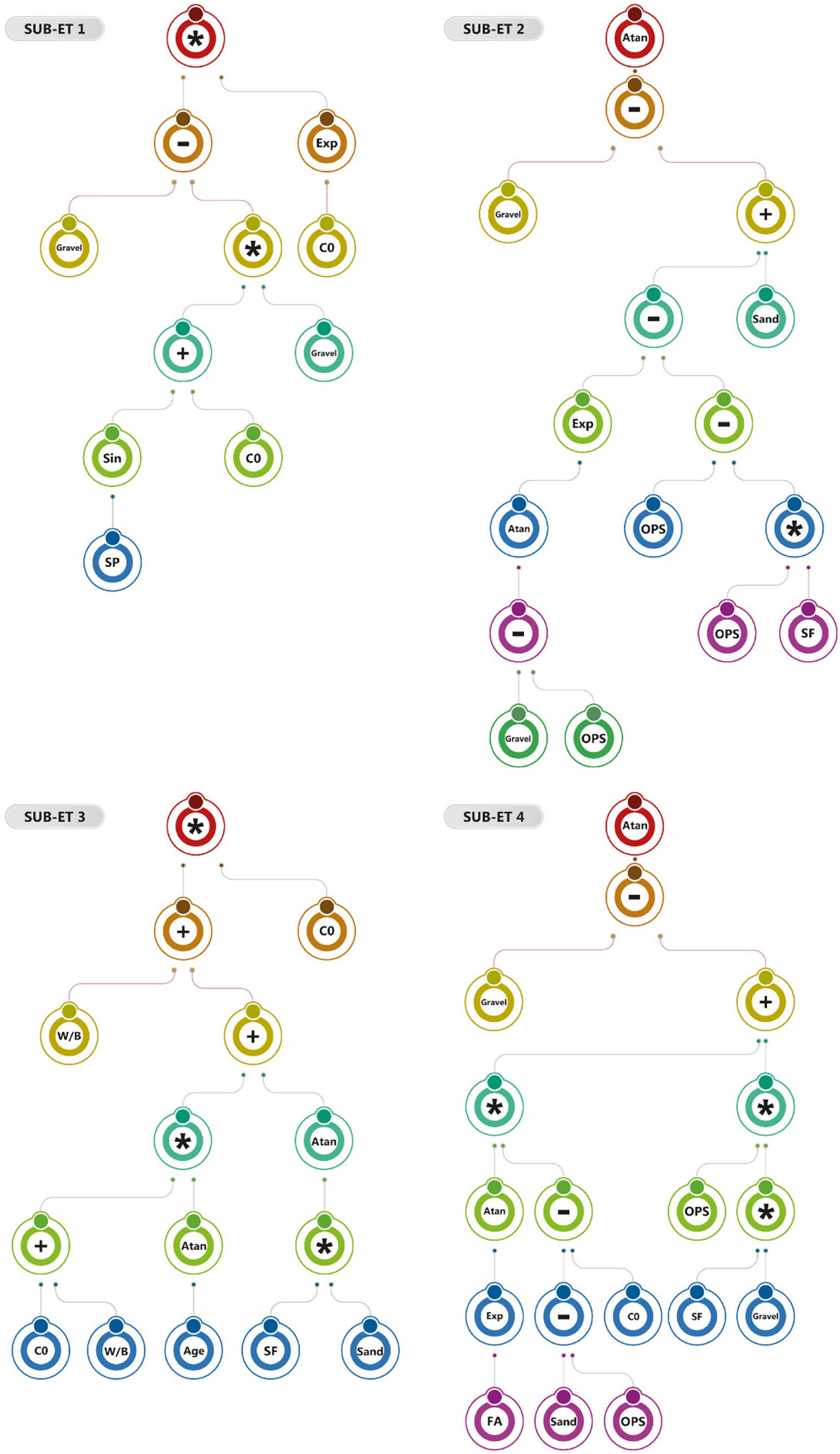

Fig. 7 *GEP*18's expression trees

Table 4 Specifications for selecting reliable models

Description	*ANFIS* models				
Name of the model	*C2*	*C3*	*C4*	*C5*	*C6*
Number of clusters	2	3	4	5	6
Number of nodes	52	72	92	112	132
Number of unknown linear parameters	20	30	40	50	60
Number of unknown nonlinear parameters	36	54	72	90	108
Total number of unknown parameters	56	84	112	140	168
Number of known parameters (training datasets)	160	160	160	160	160
Is the model reliable?	*Yes*	*Yes*	*Yes*	*Yes*	*No*

using Eq. (2), input variables were normalized in the range of $0.1 - 0.9$.

$$x_i = 0.8\frac{x - x_{min}}{x_{max} - x_{min}} + 0.1 \tag{2}$$

where x is the measured value of a parameter and x_i is the normalized value. In addition, x_{min} and x_{max} are the minimum and maximum values of variable x in the data. Note that since, in the *GEP* modeling, the effect of weight is considered, there is no need to normalize the data. It should be mentioned that in the *MLR* method, normalizing the data had a negative effect and lowered the model's performance.

Performance parameters

The developed models' performance was assessed using parameters including *RMSE*, *MAE*, and R^2 through the following equations:

$$RMSE = \sqrt{\frac{1}{n}\sum_{i=1}^{n}\left(t_i - o_i\right)^2} \tag{3}$$

$$MAE = \frac{1}{n}\sum_{i=1}^{n}\left|t_i - o_i\right| \tag{4}$$

Table 5 Statistical parameters for each *ANFIS* model

Models	Phase	R^2	*RMSE*	*MAE*
C2	Training	0.931	3.991	2.891
	Testing	0.929	4.747	3.368
C3	Training	0.948	3.594	2.803
	Testing	0.928	4.647	3.570
C4	Training	0.957	3.198	2.368
	Testing	0.937	4.689	3.462
C5	**Training**	**0.978**	**2.260**	**1.669**
	Testing	**0.942**	**4.301**	**3.439**

Bold is the best

$$R^2 = \frac{\left(n\sum t_i o_i - \sum t_i \sum o_i\right)^2}{\left(n\sum t_i^2 - \left(\sum t_i\right)^2\right)\left(n\sum o_i^2 - \left(\sum o_i\right)^2\right)} \tag{5}$$

where t is the target value, o is the output value, n is the total number of data points, and $\bar{t}$ is the mean value of targets.

In addition to high correlation, a model should present an acceptable error to be reliable. To this end, the parameter *OBJ* was used to compare the performances of different models. This parameter is a function of R^2 value, and two errors *RMSE* and *MAE* in all modeling phases using the following equation:

$$OBJ = \left(\frac{n_{tr}}{n_{all}}\frac{RMSE_{tr} + MAE_{tr}}{R_{tr}^2 + 1}\right) + \left(\frac{n_{val}}{n_{all}}\frac{RMSE_{val} + MAE_{val}}{R_{val}^2 + 1}\right) + \left(\frac{n_{tst}}{n_{all}}\frac{RMSE_{tst} + MAE_{tst}}{R_{tst}^2 + 1}\right) \tag{6}$$

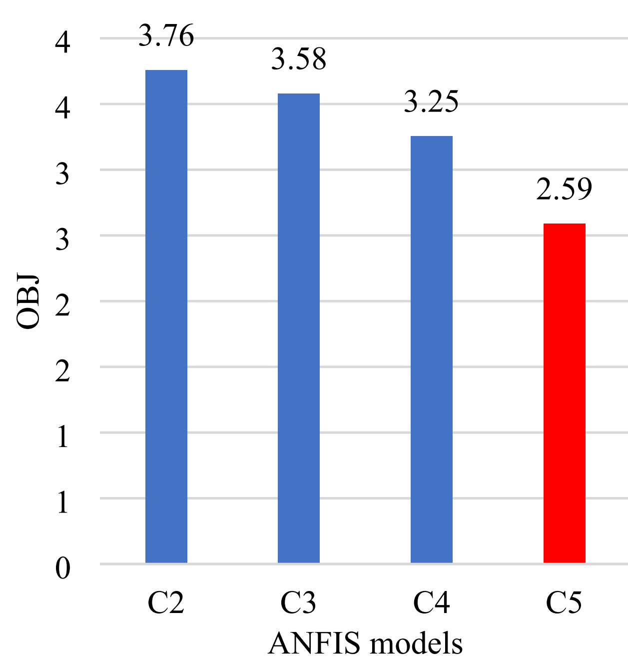

Fig. 8 The *OBJ* values for all *ANFIS* models (red bar is the best)

Table 6 Statistical parameters for each *ANN* model

Models	Phase	R^2	*RMSE*	*MAE*
*n*6	Training	0.983	2.194	1.687
	Testing	0.975	2.578	2.002
	Validation	0.943	2.606	1.922
*n*7	Training	0.983	2.034	1.485
	Testing	0.972	2.971	2.204
	Validation	0.965	3.090	2.371
*n*8	Training	0.990	1.537	1.116
	Testing	0.971	2.381	1.982
	Validation	0.937	4.861	3.557
*n*9	Training	0.984	1.906	1.375
	Testing	0.973	3.249	2.590
	Validation	0.971	2.903	2.342
*n*10	Training	0.989	1.585	1.150
	Testing	0.961	3.366	2.540
	Validation	0.941	4.543	3.195
*n*11	Training	0.990	1.578	1.069
	Testing	0.965	2.854	2.216
	Validation	0.955	3.574	2.610
*n*12	Training	0.980	2.235	1.583
	Testing	0.965	3.291	2.239
	Validation	0.974	2.790	2.196
*n*13	Training	0.991	1.460	1.043
	Testing	0.957	3.175	2.369
	Validation	0.960	3.776	2.613
*n*14	Training	0.990	1.526	1.086
	Testing	0.956	3.594	2.835
	Validation	0.962	3.668	2.775
*n*15	Training	0.980	2.262	1.584
	Testing	0.952	3.439	2.846
	Validation	0.960	3.290	2.734
*n*16	Training	0.991	1.537	1.033
	Testing	0.927	4.419	3.217
	Validation	0.931	4.359	3.395
***n*17**	**Training**	**0.994**	**1.299**	**0.774**
	Testing	**0.964**	**3.543**	**2.682**
	Validation	**0.943**	**3.390**	**2.526**
*n*18	Training	0.971	2.707	1.955
	Testing	0.954	3.344	2.816
	Validation	0.950	3.811	2.851
*n*19	Training	0.988	1.711	1.154
	Testing	0.968	2.856	2.363
	Validation	0.937	4.725	3.513
*n*20	Training	0.987	1.801	1.282
	Testing	0.951	3.294	2.545
	Validation	0.967	3.227	2.287
*n*21	Training	0.987	1.859	1.305
	Testing	0.943	4.318	3.273
	Validation	0.958	3.594	2.768
*n*22	Training	0.985	1.969	1.332
	Testing	0.931	3.736	2.935
	Validation	0.961	3.723	2.970
*n*23	Training	0.985	1.837	1.170
	Testing	0.945	4.332	3.186
	Validation	0.971	3.246	2.615
*n*24	Training	0.985	1.905	1.296
	Testing	0.943	3.650	3.053
	Validation	0.958	3.940	2.653
*n*25	Training	0.990	1.686	1.166
	Testing	0.944	3.551	2.977
	Validation	0.895	4.168	3.115
*n*26	Training	0.985	2.000	1.488
	Testing	0.905	4.895	3.551
	Validation	0.968	2.789	1.900
*n*27	Training	0.989	1.671	1.079
	Testing	0.925	5.103	3.979
	Validation	0.932	3.931	3.287

Bold is the best

where *n* is the number of patterns (data points) in the associated dataset, and *tr*, *val*, and *tst* subscripts present the training, validation, and testing datasets, respectively.

MLR model

In this study, to predict the compressive strength of $HS-LWAC$ using *MLR* method, 70% of the data were used as the training data and the remaining 30% as the testing data. The equation used in *MLR* to predict the compressive strength is as follows.

$$\begin{aligned} f_c &= 43.18 + (0.031245 * OPC) - (0.02493 * FA) - (0.38695 * SF) \\ &- (11.0925 * \frac{W}{B}) + (0.010443 * SP) \\ &- (0.0221 * Sand) + (0.025972 * Gravel) \\ &- (0.00926 * OPS) + (0.190928 * Age) \end{aligned} \tag{7}$$

Here, modeling using the *MLR* method was performed in *CurveExpertProfessional* software. *RMSE*, *MAE*, and R^2 values for the testing dataset were obtained as $9.83MPa$, 7.71, and 0.59. Furthermore, the value of *OBJ* per all the data was 8.89. The results show that the model developed using the *MLR* was not a relatively accurate prediction of the compressive strength of $HS-LWAC$.

GEP model

For an acceptable performance of the *GEP* modeling, it is necessary to set its associated parameters. 70% of the

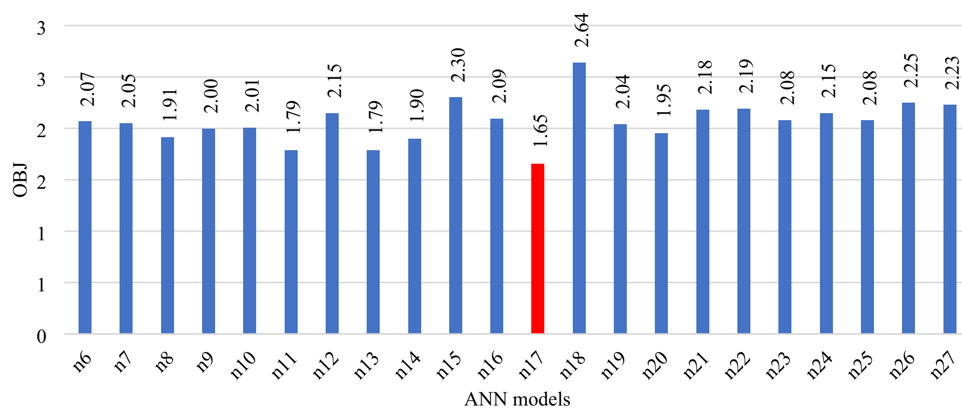

Fig. 9 The *OBJ* values for all *ANN* models (red bar is the best)

collected data were used as the training data and 30% as the validation data. Twenty different designs with different parameters were used to select the best *GEP* settings using the recommendations provided by Shahmansouri et al. (2020). Results corresponding to the performance parameters of the 20 developed models are displayed in Table 2. *OBJ* values obtained from the performance analyses of the developed models are displayed in Fig. 6, and model *GEP*18 was selected as the best model with the lowest *OBJ* value of 4.98.

GEP setting parameters used for developing *GEP*18 are reported in Table 3, and the equation obtained from this model is as follows:

$$f_c = f\left(OPC, FA, SF, {}^{W}/_{B}, SP, Sand, Gravel, OPS, Age\right) = \mathrm{ET}_1 + \mathrm{ET}_2 + \mathrm{ET}_3 + \mathrm{ET}_4 \tag{8}$$

$$ET_1 = (Gravel - (\sin SP - 5.793) * Gravel) * e^{-5.793} \tag{8a}$$

$$ET_2 = \tan^{-1}\left(Gravel - e^{\tan^{-1}(Gravel - OPC)} + OPS - OPS * SF + Sand\right) \tag{8b}$$

$$ET_3 = -5.793 * \left(W/B + (W/B - 5.793) * \tan^{-1} Age + \tan^{-1}(SF * Sand)\right) \tag{8c}$$

$$ET_4 = \tan^{-1}\left(Gravel - \tan^{-1} e^{FA} * (Sand - OPS + 5.793) - OPS * SF * Gravel\right) \tag{8d}$$

This model was then used to compare the performance of *GEP* method with other modeling methods. The expression trees of the *GEP*18 model are shown in Fig. 7.

Table 7 Statistical parameters of different models

Datasets	Statistical parameters	*ANN*	*ANFIS*	*GEP*	*MLR*
Training data	*RMSE*	1.299051	2.259774	4.858525	8.037163
	MAE	0.773868	1.668729	3.94575	6.152084
	R^2	0.993652	0.977932	0.896941	0.756924
Testing data	*RMSE*	3.543299	4.301228	6.082227	9.833508
	MAE	2.682117	3.439364	4.860466	7.709457
	R^2	0.964224	0.941744	0.898283	0.592266
All data	*RMSE*	2.180948	3.023627	5.257306	8.609786
	MAE	1.317404	2.202239	4.221363	6.614535
	R^2	0.982087	0.964507	0.895825	0.711637
	OBJ	1.653552	2.588861	4.97974	8.894597

ANFIS model

In the *ANFIS* method, 70% of the data were used for training, and 30% were used for testing the model. For all the models, the initial *FIS* was generated using fuzzy c-means (*FCM*) clustering method and then fine-tuned by employing a hybrid optimization algorithm (Pouresmaeil et al. 2022). In this method, the number of clusters first needs to be determined. To this end, all unknown model parameters (i.e., membership functions' nonlinear parameters and linear equations' coefficient parameters in the output of the rules) have a sum lower than the total number of observations (number of data utilized in the training phase). In this study, the number of clusters was considered 2 to 6, and *ANFIS* models were labeled $C2 - C6$, considering the number of clusters. After that, for models with 2, 3, 4, and 5 clusters, 56, 84, 112, and 140 unknown parameters were considered, respectively. In the *C*6 model, the sum of unknown parameters is 168, which is larger than the total number of observations or the number of training data (i.e., 160), that makes it unreliable. The modeling of each *ANFIS* structure was repeated 20 times, given the random nature of optimization problems, and the best result was saved. Further information about the *ANFIS* models can be seen in Table 4.

The best-developed models' performance parameters' values in both the training and testing phases are provided in Table 5.

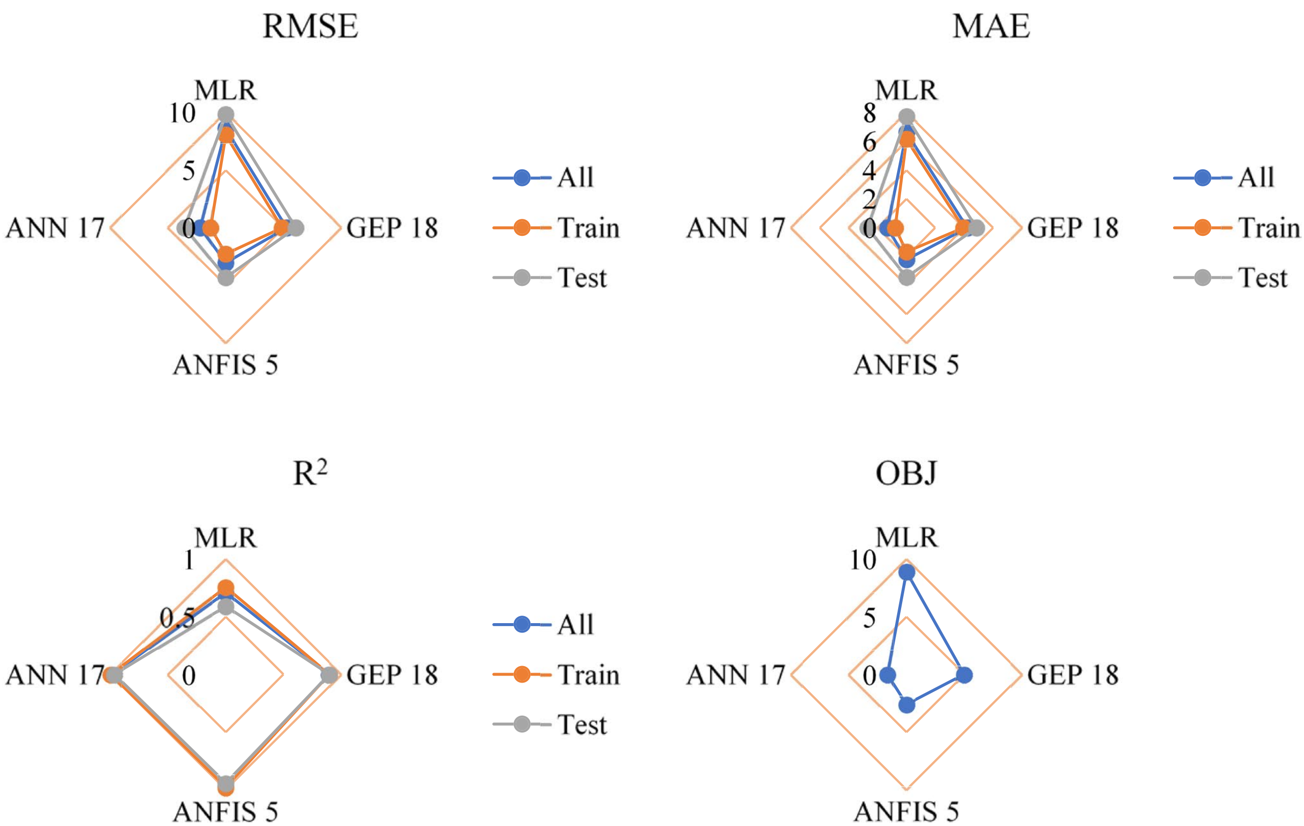

Fig. 10 Comparison between developed models in training, testing, and overall phases

The *OBJ* values of the best-developed trained model per a given cluster number are given in Fig. 8. Among the *ANFIS* models, the model with 5 clusters and an *OBJ* value of 2.59 was selected as the best model and compared with other methods. In addition, it is seen that with decreasing the number of clusters, *OBJ* increases, indicating a weaker performance of the model.

ANN model

In the *ANN* method, randomly, 70% of the data were used to train, 15% to test, and 15% to validate the model. For all the models, the Levenberg–Marquardt backpropagation algorithm was used for the network training. In the *ANN* modeling, it is necessary to specify the number of hidden layers and their neurons (Faraj et al. 2022). One hidden layer was selected for all the developed models based on the authors' experience. The number of hidden layers' neurons was selected from 6 (two-thirds of the number of input variables) to 27 (three times the number of input variables). Furthermore, the developed ANN models were named $n6-n27$, considering the number of neurons. Note that the number of neurons in the input and output layers equals the number of input and output variables (i.e., 9 and 1), respectively. The modeling of each *ANN* structure was repeated 20 times, and the best result was saved; in total, 440 *ANN* models were built. Transfer functions (*TF* s) in the hidden and output layers were of the hyperbolic tangent sigmoid type and the linear type, respectively.

The best-developed models' performance parameters' values in terms of neurons' numbers are provided in Table 6 for the training, testing, and validation phases. In addition, Fig. 9 presents the *OBJ* values of the best-constructed model per a given number of neurons for each trained model. Among all the developed models, the neural network model with 17 neurons (with the lowest *OBJ* value of 1.65) was selected as the best model and further used for comparison with other modeling methods in this study.

Results and discussion

Table 7 lists the values of performance parameters for the best-constructed models using the four employed methods. Before assessing and comparing the models, it must be ensured that no overfitting occurred in the modeling.

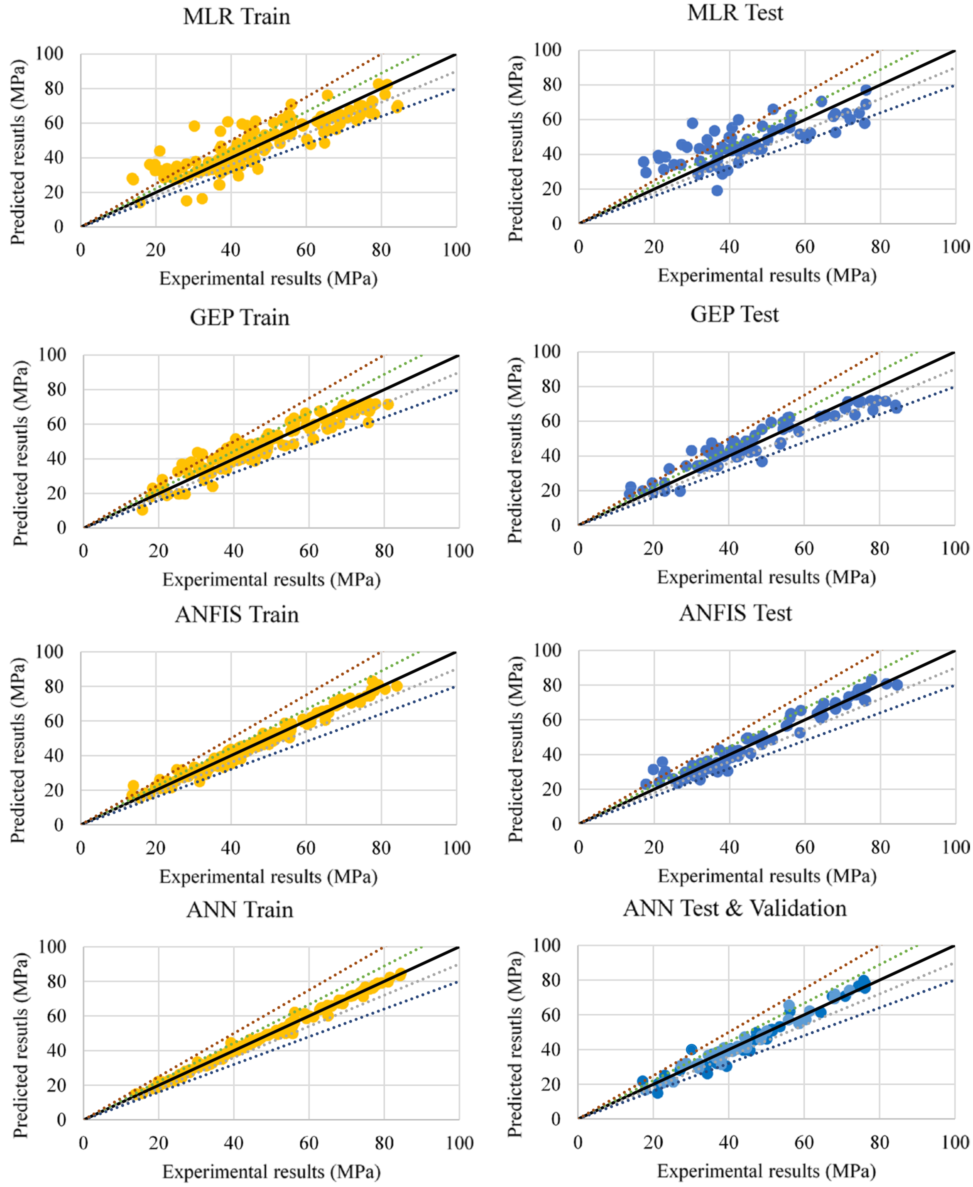

Fig. 11 Predicted f_c versus experimental results for training and testing dataset

Overfitting is a common issue in modeling using *ML*-based methods and occurs when the performance values are acceptable for the training data while they are significantly weaker for the testing data. Overfitting can be detected by comparing the four aforementioned performance parameters in the training and testing phases. As the difference in the performance parameters between the training and testing phases declines, the probability of overfitting decreases.

Considering the values reported in Table 7, no overfitting occurred in modeling using the four methods of interest. A higher R^2 value indicates a strong correlation between the experimental and prediction data of the models. As can be seen, *MLR* and *GEP* have weaker performances compared with *ANN* and *ANFIS* in both training and testing phases. In general, *ANN* has the best correlation with an excellent value of 0.982, followed by *ANFIS* with a correlation value of 0.964. Figure 10 shows the performance parameters schematically to allow better comparison. *ANN* had the lowest *OBJ* values in both training and testing phases and thus showed the best performance in predicting the compressive strength. After that, *ANFIS* and *GEP* respectively showed the next best performances, and *MLR* with an *OBJ* value of 8.89 had the weakest performance.

The predicted f_c for the training and testing datasets using the best models of the four described methods against the experimental f_c are displayed in Fig. 11. As is shown in this figure, the linear regression equation with bias zero is also provided. Lines representing the main lines' 10% and 20% errors are also drawn in the diagrams. In the *ANN* modeling, except for five points, all the other points have errors lower than 20%, which correspond to compressive strength values lower than 50 *MPa*. For f_c higher than

Fig. 12 Graphical comparison of *ANN*, *ANFIS*, *GEP*, and *MLR* models in the overall phase

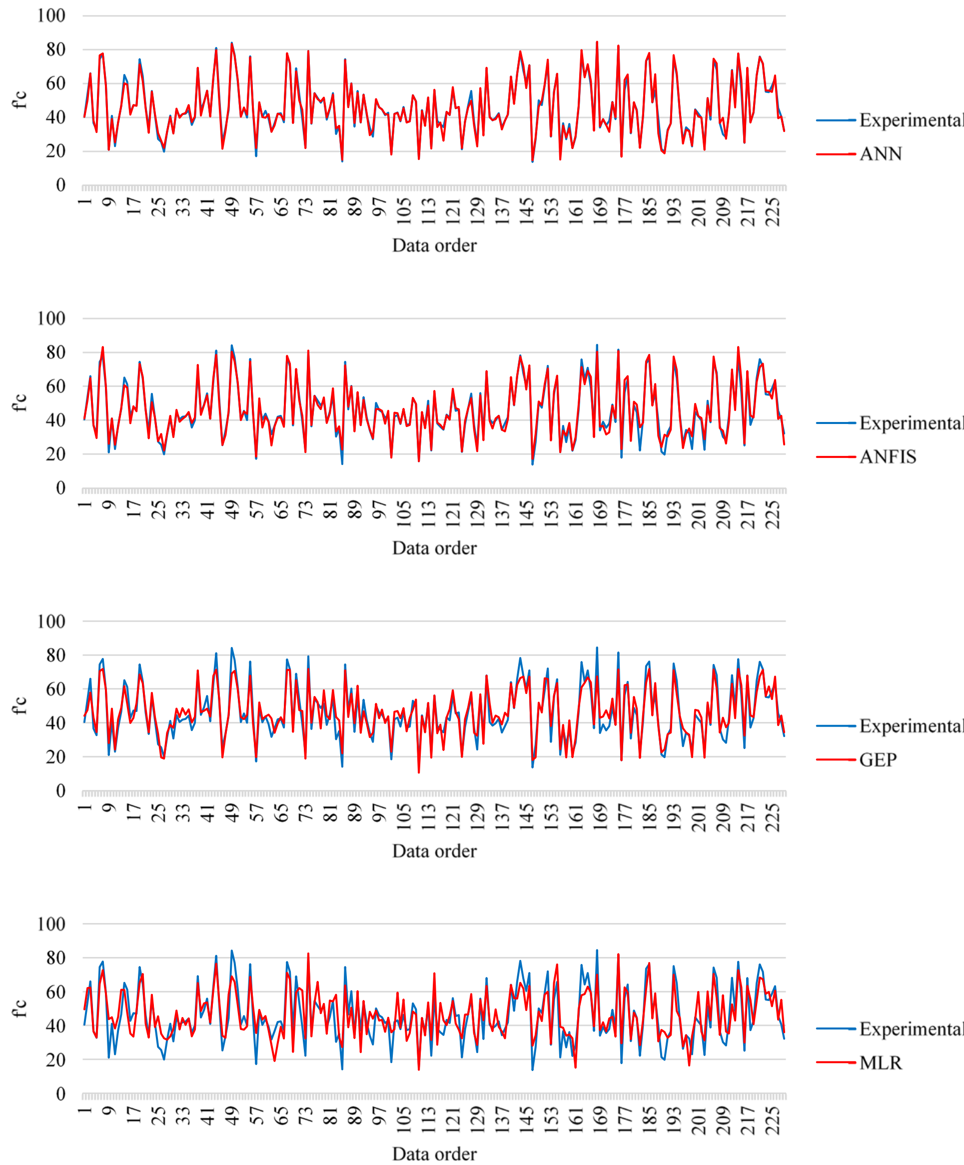

50MPa, all the points have errors lower than 20%, with only four points with errors higher than 10%. This observation indicates that the *ANN* model has an excellent performance in predicting f_c of higher strength concrete. The *ANFIS* model also had a proper performance in predicting the compressive strength at higher strength values and performed slightly weaker at lower strength values. The *GEP* and *MLR* methods, however, had weaker performances compared with *ANN* and *ANFIS* methods.

As is shown in Fig. 12, the predicted values using different models are compared with the experimental results. According to this figure, the predicted values by *ANN* are considerably close to the experimental results. In contrast, *MLR* and *GEP* models cannot satisfactorily predict the compressive, considering the reported experimental results.

For further investigation of the four developed models' performance, the predicted to experimental value ratio is illustrated in Fig. 13. This ratio is another criterion for demonstrating the models' ability to lower errors and provide a more accurate prediction. The lower the scattering of this ratio, the higher accuracy of the developed models becomes. As can be seen, the *ANN* model showed a better performance than the other models in both the training and testing phases. The mean Pre/Exp ratios of all the data for models *ANN*, *ANFIS*, *GEP*, and *MLR* are 0.998, 1.012, 1.024, and 1.064, respectively. Moreover, the lowest difference between the mean ratio and 1 for the *ANN* model demonstrates the

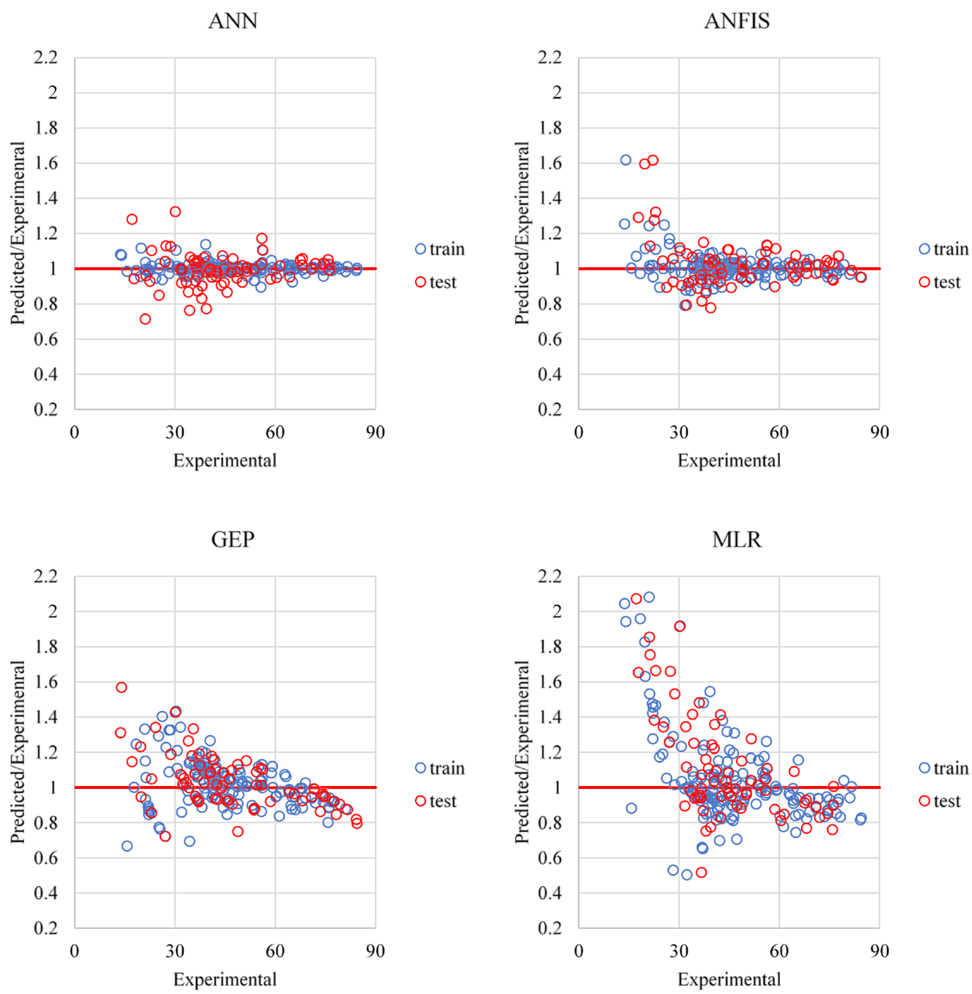

Fig. 13 Comparison of *Pre*/*Exp* ratios using *ANN*, *ANFIS*, *GEP*, and *MLR* models in train and test phases

better performance of this model. For this model, the minimum and maximum *Pre*/*Exp* ratios are 0.716 and 1.324, respectively. The worst performance pertains to *MLR*, with the minimum and maximum *Pre*/*Exp* values of 0.506 and 2.083, respectively.

Figure 14 shows the error values of the developed models in the testing phase. As can be seen, the mean error values of the *GEP* and *ANN* models are 0.03 and 0.28, respectively, which are much lower than *ANFIS* and *MLR* models' errors (i.e., 0.63 and 2.14, respectively). In addition, in the *ANN* model, the first and third quartiles are −1.85 and 2.51, respectively, indicating an interquartile range of 4.36. The corresponding values for models *ANFIS*, *GEP*, and *MLR* are 5.16, 8.04, and 13.44, respectively. A smaller interquartile range indicates greater concentration and lowers the scattering of the error data. The value of this parameter in *ANN* is 15.57, 45.77, and 67.56% lower than the corresponding values in *ANFIS*, *GEP*, and *MLR*, respectively.

The uncertainty technique inspired by Monte Carlo simulation (MCS) was employed to specify the randomness of the developed models. The prediction of the compressive strength is associated with several uncertainties (e.g., experimental uncertainty, input predictors uncertainty, and model parameters uncertainty) (Ashrafian et al. 2022). The MCS analysis was conducted for the MLR, GEP, ANFIS, and ANN models. The results of this study (e.g., median of predicted f_c, mean absolute deviation (MAD), and width of uncertainty band) are reported in Table 8. According to the table, the positive values of the average prediction error show that the f_c predicted using all approaches above are higher than the experimental values. Also, the ANN and MLR presented the lowest (20.370%) and highest (38.154%) uncertainty bandwidths, respectively.

Conclusions

Replacement of natural coarse aggregate with agricultural wastes/byproducts such as *OPS* in the *LWC* production process can reduce environmental impact and promote sustainable development. Precise prediction of *OPS* − *LWAC* compressive strength is a determinative factor

Fig. 14 Error box plot diagram of models in the testing phase

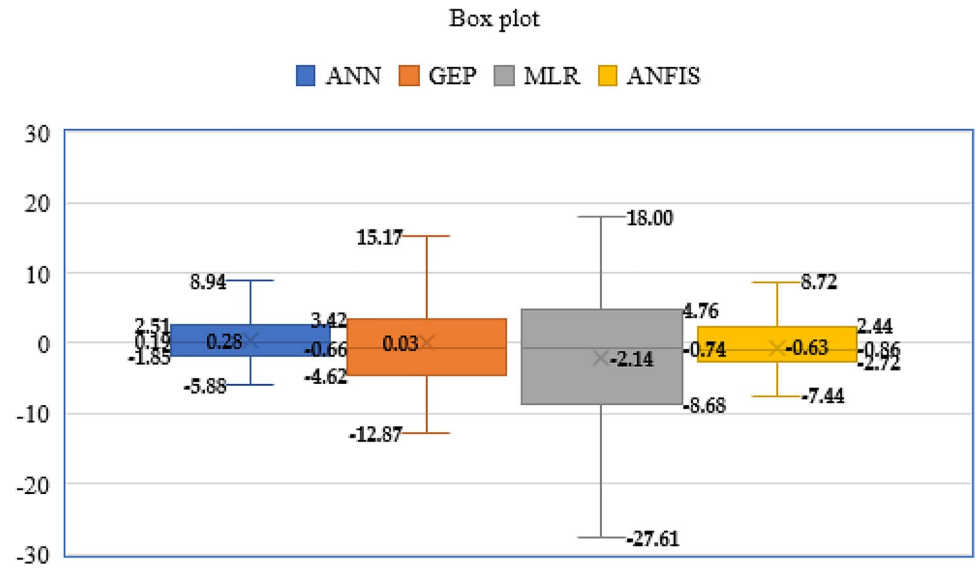

Table 8 MCS uncertainty analysis of the proposed models

Model	Median	MAD	Uncertainty (%)
MLR	62.145	27.112	38.154
GEP	53.110	19.662	29.780
ANFIS	47.416	16.553	24.020
ANN	42.800	12.573	20.370

in decision-making before the concrete field placement. The research aims to investigate if different *ML* and regression approaches can be used to predict $HS-OPS-LWAC$'s f_c. To this end, a relatively comprehensive dataset is used to develop three models, including *GEP*, *ANFIS*, and *ANN*. After that, the developed models' performance is compared to the results obtained from the regression model (*MLR*). The following conclusions can be drawn from the investigation's research results:

- According to the research results, all *ML* approaches were effectively employed to develop prediction models for the $HS-OPS-LWAC$ compressive strength.
- The suggested *ML* models outperform statistical evaluation indices such as *MAE*, *RMSE*, R^2, and *OBJ*, indicating the models' excellent abilities and potential for further/future practical application.
- The calculated correlation coefficient (R^2) for the training, testing, and validating phases of all developed models (i.e., *GEP*, *ANFIS*, and *ANN*) was greater than 0.8, indicating a good fit between model predictions and experimental data.
- The *ANN*-based model with 17 neurons with the *OBJ* value of 1.65 outperformed all developed models. Furthermore, the *ANN*-based models demonstrate better efficiency and performance than the developed *ANFIS*-based and *GEP*-based models.
- The uncertainty analysis was performed via Monte Carlo simulation (MCS) to specify the randomness of the developed models. The results show the positive values of the average prediction error. Moreover, the ANN model presented the lowest (20.370%) uncertainty bandwidth.

The findings of this study have opened up new avenues for future research using *ML* algorithms. To improve the suggested approaches' generalizability, the authors will gather a continuously updated, widely accessible, and more comprehensive database in future work. To replace missing values in the database (the input and output), advanced data pre-processing approaches such as semi-supervised learning and missing data imputation will be employed. Other *ML* approaches' effectiveness in forecasting $HS-OPS-LWAC$'s f_c will also be compared. The integrated hybrid *ML* model, which combines *ML*-based techniques with high-convergence metaheuristic optimization algorithms (e.g., Seydanlou et al. 2022, Shaswat 2021), might be studied as a feasible option to increase the concrete properties' estimation accuracy (e.g., modulus of elasticity, compressive, tensile, and flexural strengths). Finally, the suggested *ML*-based model will be integrated into construction industry systems to make $HS-OPS-LWAC$ easier to produce. However, further study in this area is necessary.

Author contribution Saeed Ghanbari: formal analysis; methodology; software; validation; original draft; visualization; review and editing. Amir Ali Shahmansouri: formal analysis; investigation; original draft; visualization; supervision; project admiration; review and editing. Habib Akbarzadeh Bengar: supervision; review and editing. Abouzar

Jafari: review and editing. All authors read and approved the final manuscript.

Data availability Data and materials will be available upon request.

Declarations

Ethical approval Not applicable.

Consent to participate Not applicable.

Consent for publication The authors consent to publish.

Competing interests The authors declare no competing interests.

References

Ahmad Zawawi MNA, Muthusamy K, Abdul Majeed APP, Muazu Musa R, Mokhtar Albshir Budiea A (2020) Mechanical properties of oil palm waste lightweight aggregate concrete with fly ash as fine aggregate replacement. J Build Eng 27:100924

Ahmed HU, Mohammed AS, Mohammed AA (2022) Proposing several model techniques including ANN and M5P-tree to predict the compressive strength of geopolymer concretes incorporated with nano-silica. Environ Sci Pollut Res. https://doi.org/10.1007/s11356-022-20863-1

Alengaram UJ, Jumaat MZ, Mahmud H (2008a) Influence of sand content and silica fume on mechanical properties of palm kernel shell concrete. In: Int conf constr build technol pp. 251–262

Alengaram UJ, Jumaat MZ, Mahmud H (2008b) Ductility behaviour of reinforced palm kernel shell concrete beams. Eur J Sci Res 23:406–420

Alengaram UJ, Muhit BAA, Jumaat MZb (2013) Utilization of oil palm kernel shell as lightweight aggregate in concrete – a review. Constr Build Mater 38:161–172

American concrete institute (1997) State-of-the-art report on high-strength concrete, ACI Committee 363 Report, pp. 92

Andrews DF (1974) A robust method for multiple linear regression. Technometrics 16:523–531

Ashrafian A, Shahmansouri AA, Akbarzadeh Bengar H, Behnood A (2022) Post-fire behavior evaluation of concrete mixtures containing natural zeolite using a novel metaheuristic-based machine learning method. Archiv Civ Mech Eng 22:101

Aslam M, Shafigh P, Jumaat MZ (2015) Structural lightweight aggregate concrete by incorporating solid wastes as coarse lightweight aggregate. Appl Mech Mater 749:337–342

Aslam M, Shafigh P, Jumaat MZ (2016a) Oil-palm by-products as lightweight aggregate in concrete mixture: a review. J Clean Prod 126:56–73

Aslam M, Shafigh P, Jumaat MZ (2016b) Drying shrinkage behaviour of structural lightweight aggregate concrete containing blended oil palm bio-products. J Clean Prod 127:183–194

Aslam M, Shafigh P, Jumaat MZ, Lachemi M (2016c) Benefits of using blended waste coarse lightweight aggregates in structural lightweight aggregate concrete. J Clean Prod 119:108–117

Aslam M, Shafigh P, Jumaat MZ (2017) High strength lightweight aggregate concrete using blended coarse lightweight aggregate origin from palm oil industry. Sains Malaysiana 46:667–675

Aslam M, Shafigh P, Jumaat MZ (2018) Drying shrinkage strain of palm-oil by-products lightweight concrete: a comparison between experimental and prediction models. KSCE J Civ Eng 22:4997–5008

Chinnu SN, Minnu SN, Bahurudeen A, Senthilkumar R (2021) Reuse of industrial and agricultural by-products as pozzolan and aggregates in lightweight concrete. Constr Build Mater 302:124172

Chou J-S, Pham A-D (2013) Enhanced artificial intelligence for ensemble approach to predicting high performance concrete compressive strength. Constr Build Mater 49:554–563

Ehteram M, Ahmed AN, Latif SD, Huang YF, Alizamir M, Kisi O, Mert C, El-Shafie A (2021) Design of a hybrid ANN multi-objective whale algorithm for suspended sediment load prediction. Environ Sci Pollut Res 28:1596–1611

Farahani JN, Shafigh P, Alsubari B, Shahnazar S, Mahmud HB (2017a) Engineering properties of lightweight aggregate concrete containing binary and ternary blended cement. J Clean Prod 149:976–988

Farahani JN, Shafigh P, Mahmud HB (2017b) Production of a green lightweight aggregate concrete by incorporating high volume locally available waste materials. Procedia Eng 184:778–783

Faraj RH, Mohammed AA, Omer KM (2022) Modeling the compressive strength of eco-friendly self-compacting concrete incorporating ground granulated blast furnace slag using soft computing techniques. Environ Sci Pollut Res. https://doi.org/10.1007/s11356-022-20889-5

Farooq F, Ahmed W, Akbar A, Aslam F, Alyousef R (2021) Predictive modeling for sustainable high-performance concrete from industrial wastes: a comparison and optimization of models using ensemble learners. J Clean Prod 292:126032

Ferreira C (2001) Gene expression programming: a new adaptive algorithm for solving problems. arXiv preprint cs/0102027

Ferreira C (2002) Gene expression programming in problem solving. In: Soft comput ind pp. 635-653.

Ghadami N, Gheibi M, Kian Z, Faramarz MG, Naghedi R, Eftekhari M, Fathollahi-Fard AM, Dulebenets MA, Tian G (2021) Implementation of solar energy in smart cities using an integration of artificial neural network, photovoltaic system and classical Delphi methods. Sustain Cities Soc 74:103149

Gholizadeh H, Fathollahi-Fard AM, Fazlollahtabar H, Charles V (2022) Fuzzy data-driven scenario-based robust data envelopment analysis for prediction and optimisation of an electrical discharge machine's parameters. Expert Syst Appl 193:116419

Hamada HM, Skariah Thomas B, Tayeh B, Yahaya FM, Muthusamy K, Yang J (2020) Use of oil palm shell as an aggregate in cement concrete: a review. Constr Build Mater 265:120357

Hoff GC (2002) Guide for the use of low-density concrete in civil works projects. HOFF CONSULTING CLINTON MS

Hornik K, Stinchcombe M, White H (1989) Multilayer feedforward networks are universal approximators. Neural Netw 2:359–366

Islam MMU, Mo KH, Alengaram UJ, Jumaat MZ (2016) Mechanical and fresh properties of sustainable oil palm shell lightweight concrete incorporating palm oil fuel ash. J Clean Prod 115:307–314

Jang J-S (1993) ANFIS: adaptive-network-based fuzzy inference system. IEEE Trans Syst Man Cybern 23:665–685

Johnson Alengaram U, Jumaat MZ, Mahmud H, Fayyadh MM (2011) Shear behaviour of reinforced palm kernel shell concrete beams. Constr Build Mater 25:2918–2927

Latif SD (2021a) Developing a boosted decision tree regression prediction model as a sustainable tool for compressive strength of environmentally friendly concrete. Environ Sci Pollut Res 28:65935–65944

Latif SD (2021b) Concrete compressive strength prediction modeling utilizing deep learning long short-term memory algorithm for a sustainable environment. Environ Sci Pollut Res 28:30294–30302

Liu K, Zou C, Zhang X, Yan J (2021) Innovative prediction models for the frost durability of recycled aggregate concrete using soft computing methods. J Build Eng 34:101822

Londhe SN, Kulkarni PS, Dixit PR, Silva A, Neves R, de Brito J (2021) Predicting carbonation coefficient using artificial neural networks and genetic programming. J Build Eng 39:102258

Maghfouri M, Shafigh P, Binti Ibrahim Z, Alimohammadi V (2017) Quality control of lightweight aggregate concrete based on initial and final water absorption tests. IOP Conference Series: Materials Science and Engineering 210(1):012022

Maghfouri M, Shafigh P, Aslam M (2018) Optimum oil palm shell content as coarse aggregate in concrete based on mechanical and durability properties. Adv Mater Sci Eng 2018:4271497

Maghfouri M, Shafigh P, Alimohammadi V, Doroudi Y, Aslam M (2020) Appropriate drying shrinkage prediction models for lightweight concrete containing coarse agro-waste aggregate. J Build Eng 29:101148

Mehta PK, Monteiro PJ (2014) Concrete: microstructure, properties, and materials. McGraw-Hill Education

Mo KH, Alengaram UJ, Visintin P, Goh SH, Jumaat MZ (2015) Influence of lightweight aggregate on the bond properties of concrete with various strength grades. Constr Build Mater 84:377–386

Mo KH, Mohd Anor FA, Alengaram UJ, Jumaat MZ, Rao KJ (2018) Properties of metakaolin-blended oil palm shell lightweight concrete. Eur J Environ Civ Eng 22:852–868

Mo KH, Thomas BS, Yap SP, Abutaha F, Tan CG (2020) Viability of agricultural wastes as substitute of natural aggregate in concrete: a review on the durability-related properties. J Clean Prod 275:123062

Mohammadi Golafshani E, Behnood A, Hosseinikebria SS, Arashpour M (2021) Novel metaheuristic-based type-2 fuzzy inference system for predicting the compressive strength of recycled aggregate concrete. J Clean Prod 320:128771

Muthusamy K, Jaafar MS, Azhar NW, Zamri N, Samsuddin N, Albshir Budiea AM, Mohd Jaafar MF (2020) Properties of oil palm shell lightweight aggregate concrete containing fly ash as partial cement replacement. IOP Conference Series: Materials Science and Engineering 849(1):012048

Parsaie A, Haghiabi AH, Latif SD, Tripathi RP (2021) Predictive modelling of piezometric head and seepage discharge in earth dam using soft computational models. Environ Sci Pollut Res 28:60842–60856

Pouresmaeil H, Faramarz MG, ZamaniKherad M et al. (2022) A decision support system for coagulation and flocculation processes using the adaptive neuro-fuzzy inference system. Int J Environ Sci Technol. https://doi.org/10.1007/s13762-021-03848-4

Rashad A (2016) Cementitious materials and agricultural wastes as natural fine aggregate replacement in conventional mortar and concrete. J Build Eng 5:119–141

Saberian M, Li J, Donnoli A, Bonderenko E, Oliva P, Gill B, Lockrey S, Siddique R (2021) Recycling of spent coffee grounds in construction materials: a review. J Clean Prod 289:125837

Sadrmomtazi A, Noorollahi Z, Tahmouresi B, Saradar A (2019) Effects of hauling time on self-consolidating mortars containing metakaolin and natural zeolite. Constr Build Mater 221:283–291

Saradar A, Nemati P, Paskiabi AS, Moein MM, Moez H, Vishki EH (2020) Prediction of mechanical properties of lightweight basalt fiber reinforced concrete containing silica fume and fly ash: experimental and numerical assessment. J Build Eng 32:101732

Seydanlou P, Jolai F, Tavakkoli-Moghaddam R, Fathollahi-Fard AM (2022) A multi-objective optimization framework for a sustainable closed-loop supply chain network in the olive industry: hybrid meta-heuristic algorithms. Expert Syst Appl 203:117566

Shadmani A, Tahmouresi B, Saradar A, Mohseni E (2018) Durability and microstructure properties of SBR-modified concrete containing recycled asphalt pavement. Constr Build Mater 185:380–390

Shafigh P, Jumaat MZ, Mahmud H (2011a) Oil palm shell as a lightweight aggregate for production high strength lightweight concrete. Constr Build Mater 25:1848–1853

Shafigh P, Jumaat MZ, Mahmud HB, Alengaram UJ (2011b) A new method of producing high strength oil palm shell lightweight concrete. Mater Des 32:4839–4843

Shafigh P, Jumaat MZ, Mahmud HB (2012a) Effect of replacement of normal weight coarse aggregate with oil palm shell on properties of concrete. Arab J Sci Eng 37:955–964

Shafigh P, Jumaat MZ, Mahmud HB, Hamid NAA (2012b) Lightweight concrete made from crushed oil palm shell: tensile strength and effect of initial curing on compressive strength. Constr Build Mater 27:252–258

Shafigh P, Mahmud HB, Jumaat MZ (2012c) Oil palm shell lightweight concrete as a ductile material. Mater Des 1980–2015(36):650–654

Shafigh P, Johnson Alengaram U, Mahmud HB, Jumaat MZ (2013a) Engineering properties of oil palm shell lightweight concrete containing fly ash. Mater Des 49:613–621

Shafigh P, Jumaat MZ, Mahmud HB, Alengaram UJ (2013b) Oil palm shell lightweight concrete containing high volume ground granulated blast furnace slag. Constr Build Mater 40:231–238

Shafigh P, Ghafari H, Mahmud HB, Jumaat MZ (2014a) A comparison study of the mechanical properties and drying shrinkage of oil palm shell and expanded clay lightweight aggregate concretes. Mater Des 60:320–327

Shafigh P, Mahmud HB, Jumaat MZ, Zargar M (2014b) Agricultural wastes as aggregate in concrete mixtures – a review. Constr Build Mater 53:110–117

Shafigh P, Mahmud HB, Jumaat MZB, Ahmmad R, Bahri S (2014c) Structural lightweight aggregate concrete using two types of waste from the palm oil industry as aggregate. J Clean Prod 80:187–196

Shafigh P, Nomeli MA, Alengaram UJ, Mahmud HB, Jumaat MZ (2016) Engineering properties of lightweight aggregate concrete containing limestone powder and high volume fly ash. J Clean Prod 135:148–157

Shafigh P, Chai LJ, Mahmud HB, Nomeli MA (2018) A comparison study of the fresh and hardened properties of normal weight and lightweight aggregate concretes. J Build Eng 15:252–260

Shahmansouri AA, Akbarzadeh Bengar H, Ghanbari S (2020) Compressive strength prediction of eco-efficient GGBS-based geopolymer concrete using GEP method. J Build Eng 31:101326

Shahmansouri AA, Yazdani M, Ghanbari S, Akbarzadeh Bengar H, Jafari A, Farrokh Ghatte H (2021) Artificial neural network model to predict the compressive strength of eco-friendly geopolymer concrete incorporating silica fume and natural zeolite. J Clean Prod 279:123697

Shahmansouri AA, Yazdani M, Hosseini M, Akbarzadeh Bengar H, Farrokh Ghatte H (2022) The prediction analysis of compressive strength and electrical resistivity of environmentally friendly concrete incorporating natural zeolite using artificial neural network. Constr Build Mater 317:125876

Shaswat K (2021) Concrete slump prediction modeling with a fine-tuned convolutional neural network: hybridizing sea lion and dragonfly algorithms. Environ Sci Pollut Res

Shishegaran A, Boushehri AN, Ismail AF (2020) Gene expression programming for process parameter optimization during ultrafiltration of surfactant wastewater using hydrophilic polyethersulfone membrane. J Environ Manage 264:110444

Sodhi AK, Bhanot N, Singh R, Alkahtani M (2021) Effect of integrating industrial and agricultural wastes on concrete performance with and without microbial activity. Environ Sci Pollut Res

Teo DCL, Mannan MA, Kurian JV (2006) Flexural behaviour of reinforced lightweight concrete beams made with oil palm shell (OPS). J Adv Concr Technol 4:459–468

Thomas BS, Kumar S, Arel HS (2017) Sustainable concrete containing palm oil fuel ash as a supplementary cementitious material – a review. Renew Sustain Energy Rev 80:550–561

Yahaghi J, Kamal NLBM, Muda ZC, Shafigh P, Beddu SB (2016) Effect of thickness on impact resistance of lightweight aggregate concrete. Int J Appl Eng Res 11:6753–6756

Zhang J, Li D, Wang Y (2020) Predicting uniaxial compressive strength of oil palm shell concrete using a hybrid artificial intelligence model. J Build Eng 30:101282